

Filtered-Guided Diffusion: Fast Filter Guidance for Black-Box Diffusion Models

Zeqi Gu
Cornell Tech

zg45@cornell.edu

Abe Davis
Cornell University

abedavis@cornell.edu

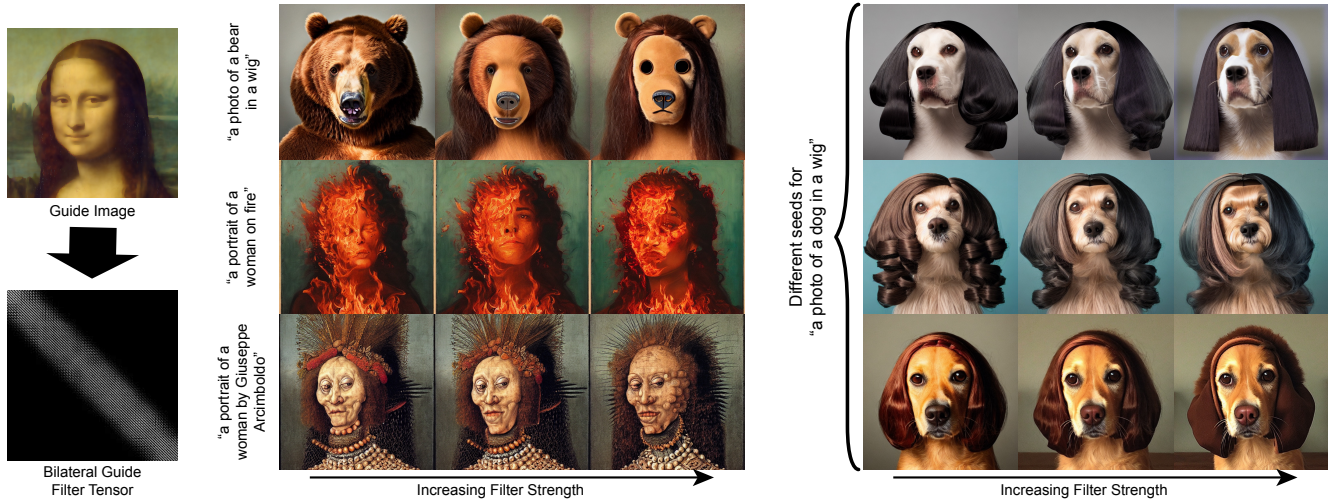


Figure 1: We present Filter-Guided Diffusion (FGD), a novel approach to guiding black-box diffusion processes based on an adaptive filter. Our method is fast, architecture-independent, and allows for continuous control over the strength of guidance. Here we use a filter derived from the guide image on the top left to guide the structure of images produced by Stable Diffusion [27]. Increasing the strength of the filter preserves more of the guide image’s structure. The middle grid of results shows the same guide filter used with three different text prompts. The grid on the right shows the same text prompt sampled with three different seeds. All of the results here show FGD as standalone guidance approach. It can also be combined with existing methods to offer finer control over the preservation of guide structure.

Abstract

Recent advances in diffusion-based generative models have shown incredible promise for Image-to-Image translation and editing. Most recent work in this space relies on additional training or architecture-specific adjustments to the diffusion process. In this work, we show that much of this low-level control can be achieved without additional training or any access to features of the diffusion model. Our method simply applies a filter to the input of each diffusion step based on the output of the previous step in an adaptive manner. Notably, this approach does not depend on any specific architecture or sampler and can be done without access to internal features of the network, making it easy to combine with other techniques, samplers, and diffusion architectures. Furthermore, it has negligible cost to performance, and allows for more continuous adjust-

ment of guidance strength than other approaches. We show FGD offers a fast and strong baseline that is competitive with recent architecture-dependent approaches. Furthermore, FGD can also be used as a simple add-on to enhance the structural guidance of other state-of-the-art I2I methods. Finally, our derivation of this method helps to understand the impact of self attention, a key component of other recent architecture-specific I2I approaches, in a more architecture-independent way.

1. Introduction

Image-to-Image translation (I2I) is the task of transforming a given image from one domain to another target domain. Since the advent of diffusion models, the most prevalent way to specify the target domain is through text

prompts. However, as target contents described by language can be realized without sticking to the original image, one of the most important question regarding translation consistency is how to maintain the original layout and structure. Many methods have been proposed recently, and they are often dependent upon model tuning [14, 35], model architecture [32], sampling methods [32, 23], or prompting scheme [9, 15], etc. We present Filter-Guided Diffusion (FGD), a simple strategy for guiding diffusion processes by making adaptive adjustments to the mean values produced at each diffusion step. FGD guides the structure of generated outputs without additional training or access to internal features of the diffusion network, making it highly portable to different architectures and complementary to other guidance strategies.

At the core of our approach are three observations. First, we can limit the diffusion process to specific frequencies by selectively replacing frequency content at each diffusion step. Second, we can adjust the amount of replacement at each step based on how likely the process is to converge on a result with desired structure, which lets us control the overall strength of guidance while keeping the diffusion process as close as possible to its training distribution. Finally, we can fit our guidance in the frequency domain to the structure of an example image using a fast linearization of the joint bilateral filter. We derive each of these observations and show that they bring the performance of black-box diffusion guidance much closer to that of the architecture-aware ones. In summary, our key contributions include:

1. We derive an black-box guidance strategy from the frequency analysis of a general diffusion process.
2. We show how the amount of guidance can be varied smoothly with our method.
3. We show quantitatively and qualitatively that our method provides a strong, fast baseline for guidance, and that it can also be used as a plug-in for various other I2I diffusion methods offering improved structural control.

2. Related Work

2.1. Image-to-Image Translation

I2I has been an active area of research for long. Early work on Laplacian Pyramid Blending [2] focused on applying transferring detail from a target image to the structure of a source, where detail and structure were distinguished by respective bands in the frequency domain. Later work used generative adversarial networks to learn translation mappings from distributions of training data, but such methods usually required images from both domains [11, 36, 21], training on the specific tasks [13], or difficult inversion to the latent space [34, 12, 3, 22].

Besides image-based guidance, many approaches now use text to guide the translation. Diffusion models have proven especially powerful when combined with LLMs [27, 19, 26, 28], replacing the need for image data representing the target domain at runtime. Our work builds on this approach by adding a convenient and very general way to condition on the structure of a guide image. Some methods, like DiffEdit [6], focus on deriving and using masks (e.g., from text prompts) to determine what parts of an image the diffusion process should be allowed to change. Their direction of localizing editing region and preserving the background is somewhat orthogonal to ours.

2.2. Architecture-Independent Guided Diffusion

As pre-trained large diffusion models often lack guidance besides text, finer control over the generation process has become an important goal. One of the earliest works in this space was SDEdit [18], which starts the reverse diffusion process from the result of applying a partial forward process to some guide image. Like our approach, SDEdit is architecture-independent, which has made it a common baseline for guided diffusion. Another architecture-independent approach is ILVR [4], which effectively conditions the generation of new images on a downsampled version of the guidance image. Our method can be seen as an extension of this approach where we condition on the edge-aware structure of an image and make the strength of this conditioning adaptive.

2.3. Architecture-Dependant Guided Diffusion

Recent and concurrent methods have explored architecture-dependent strategies for guidance. Namely, Plug-and-Play (PnP) [33] and P2P0 [23], which are very similar approaches based on the attention modules of Stable Diffusion [27]. They first invert the guide image back to noise via DDIM [29] to acquire the features of the guide image in the diffusion process. They then inject these features into the model when generating the final output for a given text prompt. This approach preserves structure better than SDEdit, but is tied to a specific architecture and sampling method (Stable Diffusion and DDIM). The use of DDIM also limits the ability to sample from diverse results, as the sampling strategy itself is used as a key component of guidance. In terms of preserving structure, this kind of architecture-aware approach has a distinct advantage over methods like ours that treat the network as a black box, yet our results suggest this advantage may be smaller than previously assumed.

3. Diffusion Background

We begin with a review of the general diffusion process on which our approach is based. Our approach should work on any model using a similar process—even, as we show,

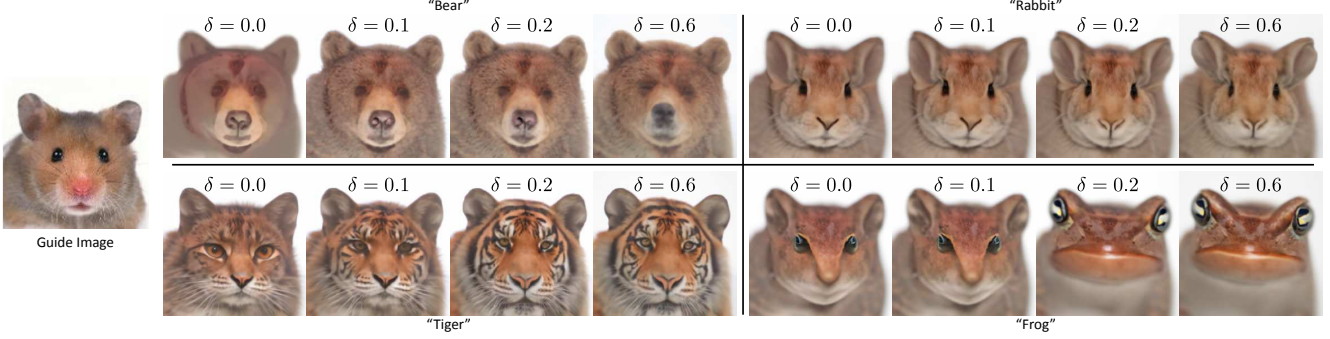


Figure 2: **FGD on GLIDE** Our method allows one to control the amount of guidance. Here we see results for different text prompts and guidance detail parameters. These results were produced with GLIDE using DDPM and $t_{stop} = 50$. We notice that when the text prompt is less likely given a guidance image, this tends to result in more modal, less continuous variation with δ . We observe this in the case of the rabbit, which is expected to have much larger ears, and the frog. In the case of the frog, the mode switches suddenly when the mouse’s ears can be explained as eyes. The bear and tiger have more continuous transitions, as they are more visually similar to begin with.

models like Stable Diffusion [27] that operate on a latent image space.

Forward Process: The forward diffusion process takes a sample $x_0 \sim q(x_0)$ from our data distribution and iteratively mixes it with Gaussian noise. We can describe this process in terms of consecutive steps x_{t-1} and x_t :

$$q(x_t|x_{t-1}) := \mathcal{N}(\sqrt{\alpha_t}x_{t-1}, \beta_t) \quad (1)$$

where $\alpha_t = 1 - \beta$. Unrolling this equation gives:

$$q(x_t|x_0) := \mathcal{N}(\sqrt{\tilde{\alpha}_t}x_0, 1 - \tilde{\alpha}_t) \quad (2)$$

where $\tilde{\alpha}_t = \prod_{i=1}^t \alpha_i$. We can interpret Eq. 2 as a linear combination of the initial data sample and noise $\mathbf{z} \sim \mathcal{N}(0, 1)$ drawn from a standard normal distribution:

$$x_t = \underbrace{(\sqrt{\tilde{\alpha}_t})}_{\text{signal strength}} x_0 + \underbrace{(\sqrt{1 - \tilde{\alpha}_t})}_{\text{noise strength}} \mathbf{z} \quad (3)$$

Eq. 3 lets us interpret x_t as a noisy measurement of a signal x_0 , where our signal strength is $\sqrt{\tilde{\alpha}_t}$ and our noise strength is $\sqrt{1 - \tilde{\alpha}_t}$. This interpretation helps to frame the reverse process in terms of denoising.

Reverse Process: The reverse process is meant to approximate repeated sampling from the posterior distribution $q(x_{t-1}|x_t)$, which we approximate as Gaussian:

$$q(\bar{x}_{t-1}|\bar{x}_t) \approx \mathcal{N}(\mu_\theta(\bar{x}_t), \sigma_t^2) \quad (4)$$

To perform this sampling, we need to estimate the means $\mu_\theta(\bar{x}_t)$ (and optionally, variances σ_t^2) associated with each reverse step. These estimates are derived from a network

ϵ_θ , which is usually trained to estimate the noise $\epsilon_\theta(\bar{x}_t)$ associated with a given \bar{x}_t (i.e., the value of \mathbf{z} from Eq. 3 corresponding to input \bar{x}_t)¹. Taken together with the input \bar{x}_t , this also yields a prediction s_t of the denoised input signal \bar{x}_0 at each step. Here, writing out the connection between our network’s input \bar{x}_t , its output $\epsilon_\theta(\bar{x}_t)$, and the intermediate denoised predictions s_t helps to connect our reverse process with the forward one:

$$\bar{x}_t = \underbrace{(\sqrt{\tilde{\alpha}_t})}_{\text{signal strength}} s_t + \underbrace{(\sqrt{1 - \tilde{\alpha}_t})}_{\text{noise strength}} \epsilon_\theta(\bar{x}_t) \quad (5)$$

This connection informs how ϵ_θ is usually trained—by applying Eq. 3 to training data and predicting \mathbf{z} . In practice, an iterative approach to estimating \bar{x}_0 performs better, where the network is used to approximate the means $\mu_\theta(\bar{x}_t)$ of Eq. 4 at each step:

$$\mu_\theta(\bar{x}_t) = \frac{1}{\sqrt{\alpha_t}} \left(\bar{x}_t - \frac{\beta_t}{\sqrt{1 - \tilde{\alpha}_t}} \epsilon_\theta(\bar{x}_t, t) \right) \quad (6)$$

We refer to [10] for the derivation of Eq. 6, which is combined with Eq. 4 to compute \bar{x}_{t-1} at each step.

3.1. Black-Box Diffusion

The training distribution for a given diffusion model is determined by the forward process used in training. We derive our approach directly from this process, which is what makes it so transferable to different architectures. We assume only that the variance schedule used in training (i.e.,

¹Some variations of diffusion predict the means $\mu_\theta(\bar{x})$ or denoised images s_0 directly. Here we follow the approach described in [10].

the α_i 's and β_i 's) is either known or that it can be estimated at run time, and that we are free to observe and modify the input to ϵ_θ at each step of our guided reverse process. These are very general assumptions, which makes our method widely applicable.

4. Method

We begin by proposing a definition of guidance in terms of some input guide image x_g and filter \mathbf{f} . At a high level, the guide filter \mathbf{f} defines the properties we want to guide, and the filtered guide image $\mathbf{f}(x_g)$ tells us what values those properties should take. More specifically, we formulate guidance as control over generated sample images \hat{x}_0 such that:

$$\mathbf{f}(\hat{x}_0) \approx \mathbf{f}(x_g) \quad (7)$$

A trivial solution to this guidance criteria would be to set $\hat{x}_0 = x_g$. However, this solution leaves no room for variation that can be used to satisfy other goals (e.g., diverse results and text-based guidance). To be useful, we need to balance our guidance goal against the decisions of our diffusion model. Our approach will follow one basic design principle: to intervene in the diffusion process as little and gradually as possible such that Eq. 7 is satisfied. This principle ensures that we keep our guided process as close to our original training distribution as possible. We derive our method from this principle under the limiting assumption that \mathbf{f} can be approximated as a linear function.

4.1. Adaptive Filtering

If the guide filter \mathbf{f} is linear then variation within its null space will have no effect on Eq. 7. As such, a less trivial solution to Eq. 7 replaces only those parts of our unguided result \bar{x}_0 that fall outside of this null space:

$$\hat{x}_0 = \bar{x}_0 - \mathbf{f}(\bar{x}_0) + \mathbf{f}(x_g) \quad (8)$$

Here it is worth noting that, given appropriate choices of \mathbf{f} , Eq. 8 can be reduced to older training-free I2I methods like Laplacian blending [2] or Hybrid Images [20].² The downside to this kind of solution is that it offers no opportunity for the diffusion process to compensate or adapt to our added guidance. We can provide such an opportunity by enforcing guidance more gradually at each step of the reverse process. We first define the guidance vector \mathbf{d}_t associated with step t as the filtered difference between $\mu_\theta(\hat{x}_t)$ and our target:

$$\mathbf{d}_t = \mathbf{f}(x_g) - \mathbf{f}(\mu_\theta(\hat{x}_t)) \quad (9)$$

Adding \mathbf{d}_t to each \hat{x}_t results in a much more gradual application of guidance, as the magnitude of \mathbf{d}_t at each step is limited by the scheduled variance associated with that step.

²Here, these methods would be blending the output of unguided diffusion with our guide image.

We scale \mathbf{d}_t by an adjustable factor λ_t to further control the strength of guidance.

$$\hat{x}_{t-1} = \underbrace{\mu_\theta(\hat{x}_t) + \sigma_t^2 \mathbf{z}}_{\text{same as Eq. 4}} + \underbrace{\lambda_t \mathbf{d}_t}_{\text{adaptive adjustment}} \quad (10)$$

Here, setting $\lambda_t = 1$ would fix the filtered frequencies to their value in the guide image, effectively removing control of all filtered frequencies from the network. This has two problems. The first is that \mathbf{d}_t is likely to push our diffusion process away from its training distribution for most diffusion steps. To see this, note from Eq. 3 that each x_t is itself distributed with variance no less than $1 - \tilde{\alpha}_t$, which is likely much higher than the variance of our filtered guide image for most of the diffusion process. The second problem with setting $\lambda_t = 1$ is that it places rather strict limits on the network's ability to synthesize new content. To deal with the first problem we let λ_t scale with the expected signal strength $\sqrt{\tilde{\alpha}_t}$ from Eq. 3, which helps ensure that any signal we add at a given step will be of magnitude less than or equal to that of a plausible training image. This keeps our filtered frequencies in-distribution, but does not yet address the second problem; simply setting $\lambda_t = \sqrt{\tilde{\alpha}_t}$ would still effectively treat Eq. 7 as a hard constraint by the end of the diffusion process. To relax this, we let λ_t scale with $\hat{\mathbf{d}}_t$, the mean pixel magnitude in \mathbf{d}_t :

$$\lambda_t = \min\left(\frac{\hat{\mathbf{d}}_t}{\delta}, 1\right) \cdot \sqrt{\tilde{\alpha}_t} \quad (11)$$

This results in gradually reducing guidance when the process appears on track to match our guide image. The detail parameter δ controls how much freedom we give the network to wander from the guide structure throughout this process. We typically stop applying guidance some number of steps t_{stop} before the end of inference, after which the network has usually settled into a new mode. Fig. 4 shows the behavior of different δ applied to GLIDE, as well as the convergence of the network after step t_{stop} . Fig. 1 shows results with Stable Diffusion [27], with all filter parameters fixed except for δ , which decreases from left to right for each example.

4.2. Filter Design

The success of our approach hinges on guiding the diffusion process while also keeping it close to its training distribution. Our adaptive scaling of adjustments helps to balance these goals, but if we interpret the values being adjusted as a product of the process described in Eq. 3, our strategy still assumes that each adjustment $\lambda_t \mathbf{d}_t$ will impact the "signal" signal portion of these values more than the corresponding

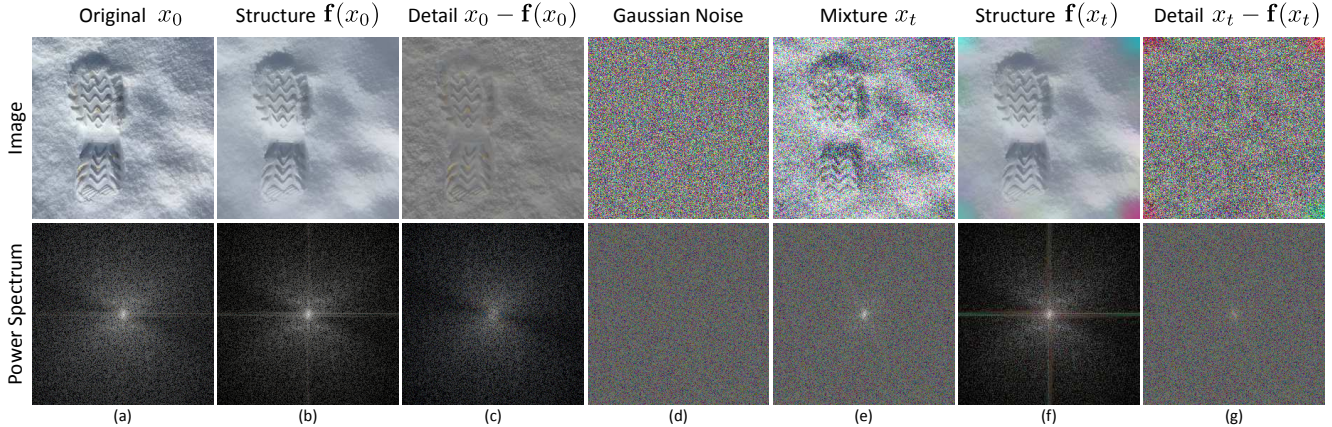


Figure 3: **Signal Strength, Diffusion, & Filtering** Our guide filter f separates images into guided structure frequencies and unguided detail frequencies. Column (b) shows the filtered structure of a guide image, which is dominated by low frequencies, while column (c) shows the residual detail. Forward diffusion mixes broad-spectrum Gaussian noise (d) with images. Natural images statistics have higher energy at low frequencies, resulting in higher SnR at these frequencies of our mixture (e). For this reason, we see the structure component of our mixture (f) change much less than our detail component (g). Our method takes advantage of this observation to guide diffusion without directing network inputs away from the training distribution.

“noise” portion. Put another way, it assumes that the signal-to-noise ratio (SNR) of our filtered content should be higher than that of the content we leave for the network to generate. Fortunately, natural image statistics make this simple to achieve. Gaussian noise is broad spectrum, while natural images have an amplitude spectrum that scales roughly with inverse frequency [8, 30]. This means that, in general, low-pass filters (e.g., a Gaussian blur) make good guide filters. An even better choice of filter is one based on the joint bilateral [7, 24], which yields a low-pass filter that preserves edges from a guide image (see Fig. 3). The results shown in this paper and most of the results in our supplemental use a joint bilateral filter based on the guide image x_g .

4.3. Fast Bilateral Tensor

Running a joint bilateral filter on 3-4 channel images can be slow in general. There are various approximations that decrease computation time, but the small image size of current diffusion models (e.g., $64 \times 64 \times c$ for GLIDE and Stable Diffusion) makes it possible to compute the exact filter extremely efficiently by packing the filter coefficients into a single tensor operation that can be applied to the entire image. The size of this tensor does not scale with the number of channels, making it suitable for latent spaces like the one used in Stable Diffusion [27], and the time to evaluate does not depend on kernel size, so arbitrary spatial and value standard deviations are equally fast. Computing the filter this way takes milliseconds in our implementation, adding negligible cost to the diffusion process.

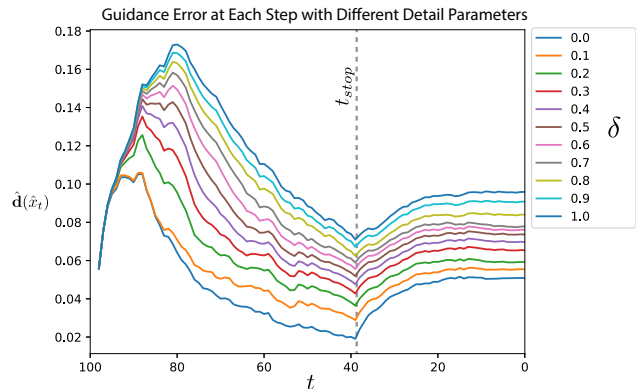


Figure 4: $\hat{d}_{\hat{x}_t}$ with Different $\delta \hat{d}_{\hat{x}_t}$ over different time steps for GLIDE diffusion guided by the mouse image using our method with the text prompt “bear”. Each line shows the adaptive behavior with a different value of δ . Guidance stops at $t = 40$, after which we see the network converge on a mode that has adopted much of the guide image’s structure. Higher values of δ let results differ more from the guide image, which tends to result in more detail added by the network.

Recap of Changes: Note that the only actual change we have made to the diffusion process is that Eq. 4 from the unguided process is replaced with Eq. 10, which adds a scaled update at each step. This can be implemented with few lines of code.

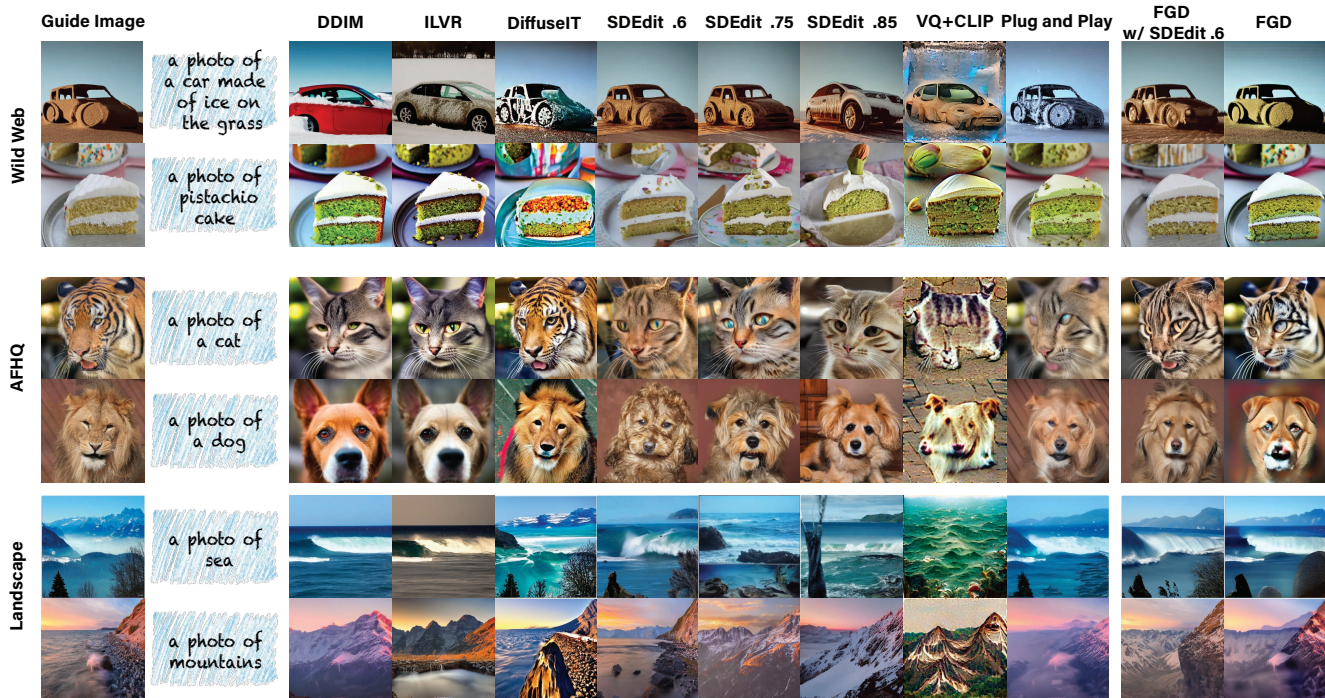


Figure 5: **Qualitative Comparison** We use Wild Web, AFHQ and Landscape to compare with 3 groups of methods: (1) strong GAN benchmark – VQ+CLIP, (2) diffusion baselines – DDIM and SDEdit with different hyper-parameters, and (3) latest state-of-the-art diffusion methods – PnP and DiffuseIT. As seen on the right, our simple method (FGD with PLMS and DDIM inversion; FGD plugged into SDEdit of strength 0.6) is comparable with strong, architecture and sampling dependent ones such as PnP.

5. Implementation & Test Parameters

To use FGD, we only need access to the inputs and outputs of each step, as well as the $\sqrt{\bar{\alpha}_t}$ used to train the model. At each step, we take the current means, apply our joint bilateral tensor, and measure \mathbf{d}_t , the difference of this result with the filtered guide image. $\mathbf{d}_{\bar{x}_t}$ is just the L_1 norm of this difference normalized by the number of pixel values in our image. We then use Eq. 11 to calculate λ and Eq. 10 to update our means.

Current top-performing Text-to-Image diffusion models can be divided into 2 types based on what space the diffusion is done in: pixel space or some latent space. The former includes the series of GLIDE [19] and DALL-E [26], and the latter includes Stable Diffusion [27]. We test our method with models of both types that have publicly available pre-trained weights, namely GLIDE and Stable Diffusion v1–4. Both models perform diffusion in a 64×64 resolution image space, then upsample to 256×256 and 512×512 respectively. We also tested FGD with different sampling methods: DDPM [10], DDIM [29] and PLMS [17]. As shown in other works, DDIM and PLMS tend to result in structure closer to the guide image, while

DDPM and SDEdit [18] offer more diverse results. Most of our experiments were run on an NVIDIA RTX A6000. Default parameters used for testing each method are given in Table 1, but as we show in our results and supplemental, changing t_{stop} and δ allows one to explore different balances of network-provided detail and guide image structure.

6. Evaluation

We conduct extensive experiments on 2 existing datasets well suited for I2I translation tasks: Animal Faces-HQ (AFHQ) [5] and Landscape Pictures [1]. AFHQ consists of faces of various animals including cats, dogs, tigers, foxes, etc., and Landscape consists of 6 types of natural scenes: mountain, desert, sea, beach, island and Japan. For source (required by DiffuseIT [15]) and target text prompts we automatically generated by concatenating category words with the template phrase "a photo of". To further diversify test cases, we created *Wild Web* that comprises of 168 diverse text-image pairs. All images were collected from the Internet with manually added captions. For more details please refer to the supplemental.

Method	Model	t_{start}	t_{stop}	δ	σ
DDIM	SD v1-4	50	10	0.05	5, 0.35
PLMS	SD v1-4	50	10	0.05	5, 0.35
SDEdit	SD v1-4	50	10	0.05	5, 0.35
DDPM	SD v1-4	50	25	0.2	5, 0.35
DDPM	GLIDE	100	50	0.6	3, 0.2

Table 1: Hyper-parameters. Our method needs tuning on 5 variables: the start (t_{start}) and end time (t_{stop}) of the filtering, the structure difference control (δ), and the spatial and value standard deviation of the bilateral filter (the first value in σ is for spatial and the second is for value). Since PLMS [17] is the default sampler of Stable Diffusion [27], we call its combination with our method as “FGD” or “FGD (stand)alone”.

6.1. Qualitative Results

We first demonstrate that our method can help guide generation in the pixel space, as shown in Fig. 2, the mouse guide image is successfully transformed into different animals with different extent of structure similarity guided by δ . Then we show that joint bilateral guide filter has a similar effect even when applied in the encoded feature space of Stable Diffusion [27], which makes sense as the latent space still preserves spatial information such as structure and layout of the input image. As shown in Fig. 5, our method alone, or a bare minimum of it plugged into SDEdit [18], already match or surpass many benchmarks with minimum time cost. In Fig. 6 we show more results of both content and style translation with FGD alone. Our method can also be combined with nondeterministic samplers to provide plausible results of great variety. As shown in Fig. 1 and 7, with different δ the images can fall into different modes that preserve different amounts of guide structure.

6.2. Quantitative Results

For quantitative measurements, we randomly select 335 text-images pairs from Landscape [1], 48 from AFHQ cat subset [5] (with the text prompt always being “a photo of a dog”), and use all 168 from the Wild Web. We evaluate along 2 competing dimensions: (1) whether text guidance was satisfied, and (2) whether the structure of the input image is preserved. We measure text guidance with CLIP cosine similarity [25], which is the cosine distance between the feature of the edited results and the feature of the text prompt. A higher value suggest a more complete translation. We measure structure preservation Structure Dist [31] with a pre-trained vision transformer. A lower score on Structure Dist means that the structure of the edited image is more similar to the input image.

As shown in Fig. 8, our method always significantly re-



Figure 6: **Results of Standalone FGD** Our method by itself is able to translate images to different styles, objects, and even allows satisfactory local editing.

duces the structure difference between the guide image and the output, at sometimes a small sacrifice of text alignment. However, the improvement on structure consistently outweighs the semantic misalignment when added to weaker baselines like SDEdit. For stronger architecture-dependent baselines like PnP, our method tends to bring the generation distribution to a different mode that preserves more structure. Fig. 9 further illustrates these effects. It is not surprising that the improvement of one metric would lead to worse behavior on the other since these two metrics are generally

Base Method	Sampling w/o FGD	Sampling w/ FGD	Sampling Diff	Total w/o FGD	Total w/ FGD	Total Diff
DDIM	4.314	4.376	0.062	21.165+52.013	21.616+52.013	0.451
PLMS	4.332	4.475	0.143	19.239+52.013	22.056+52.013	2.817
SDEdit .6	2.602	2.676	0.074	17.193	19.861	2.668
SDEdit .75	3.185	3.273	0.088	17.863	20.471	2.608
SDEdit .85	3.594	3.675	0.081	18.179	20.953	2.774

Table 2: Added Computation Cost of FGD (in seconds). FGD adds negligible time to most of the methods. While “Sampling” refers to only the generation process, “Total” includes not only that but also all pre-computations such as loading required information. The 52.013s added in the first two rows is the time of using DDIM to invert the image back to the latent space. Note that DDIM inversion is optional for all samplers and we chose to use them for more deterministic evaluation. As SDEdit encodes the image stochastically, it does not have this overhead. The largest computational cost added by FGD comes from the construction of the fast bilateral tensor, which makes the “Total Diff” a larger value than “Sampling Diff”.

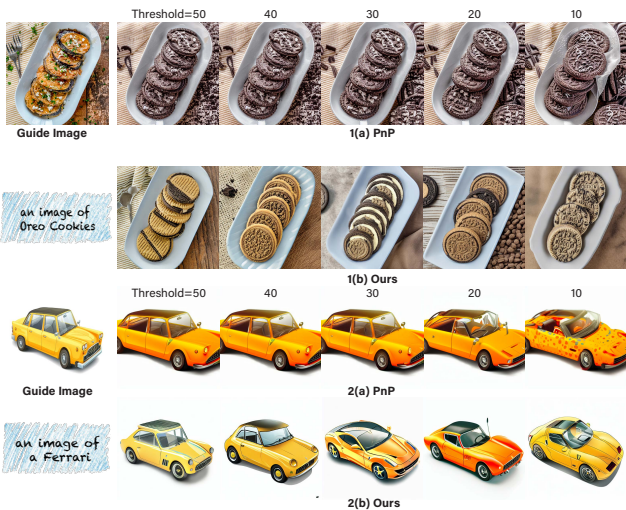


Figure 7: **Diversity Comparison** FGD produces diverse results when used with nondeterministic methods, such as SDEdit as shown above. Although one hyper-parameter of PnP, the feature injection threshold, controls the translation similarity to some degree, it essentially lacks the versatility due to being bounded with DDIM.

at odds. In this scenario, our model’s contribution is the ability to provide diverse alternative without any training and almost no overhead.

In Table 2 we compare the runtime of different existing methods with and without FGD, averaged over all quantitative comparison data. Averaging over all 5 variations, our method adds 0.089 seconds to the sampling and 2.263 seconds to the entire generation process. The total time of PnP [32] (including DDIM inversion, feature saving and reading, and sampling) is 193.917 seconds, which is $9.763\times$ that of SDEdit 0.6 with FGD, and $2.618\times$ that of PLMS with DDIM inversion and FGD.

6.3. Ablation

To study how our results are influenced by different parameters, we conduct ablation studies on different filter setups as shown in Fig. 10. The superiority of our chosen values is supported by the fact that their results (shown in black) are closest to the bottom right. The comparison with ILVR [4] here shows that a bilateral filter indeed preserves the structure better than a gaussian filter. We will provide ablations on other hyperparameters in the supplemental.

7. Discussion

7.1. Relation to Attention Map Replacement

Other concurrent strategies [33, 23] have shown empirically that replacing the attention map used in a diffusion architecture with that of the guide image (self-attention) can serve to guide the generated structure. Here we see an interesting connection with our approach. The joint bilateral, which we use as our primary guide filter, is designed to estimate local means for edge-aware denoising by mixing pixels in a target image that share similar values in a guide image. This builds on the assumption that neighboring pixels with similar values can be treated as noisy measurements of the same mean. Self-attention works in a similar manner when attention maps are derived from a denoising network. Recall that our network is trained to estimate x_0 (or a quantity analogous to it) from a noisy measurement x_t at each step, where x_t is modeled as normally distributed according to Eq 2. This amounts to estimating the mean of a noisy measurement at each pixel. We can therefore think of the maps used in self-attention as a learned variant of the joint bilateral. Or, similarly, we can think of FGD with a bilateral tensor as a more tunable fast linear architecture-independent approximation of self-attention.

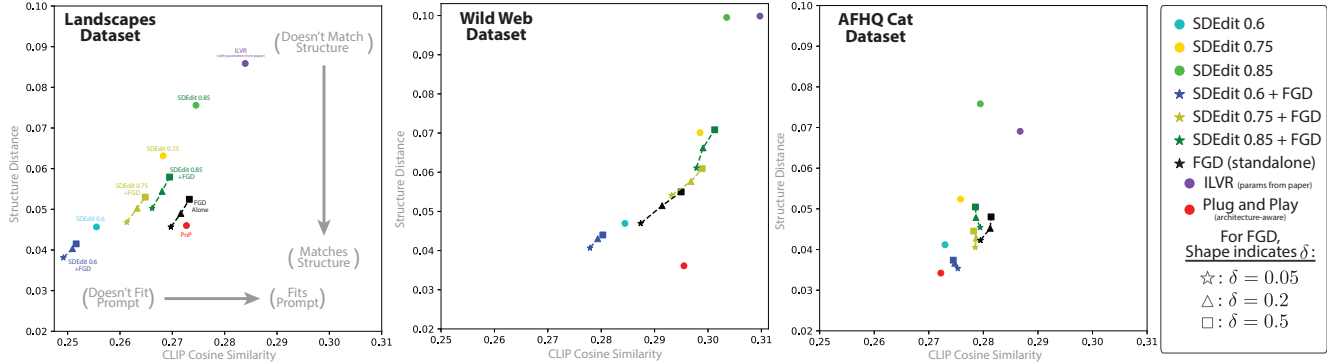


Figure 8: **Numerical Evaluation** The goal is to balance achieving higher CLIP similarity score with as small Structure Difference. There is no perfect metric for evaluating this balance, but methods that perform well should be near the bottom right corner of each. FGD successfully “pulls down” weaker methods for all 3 datasets. We connect the results of FGD using δ 0.05, 0.2, and 0.5 with dash lines and show that our δ indeed provides an effective control over image structure. The number right after “SDEdit” represents the value of its “strength” hyperparameter. Note DiffuseIT does directly optimization on the 2 metrics shown, therefore it achieves top numerical results yet is not qualitatively as satisfactory (e.g. Fig. 5).

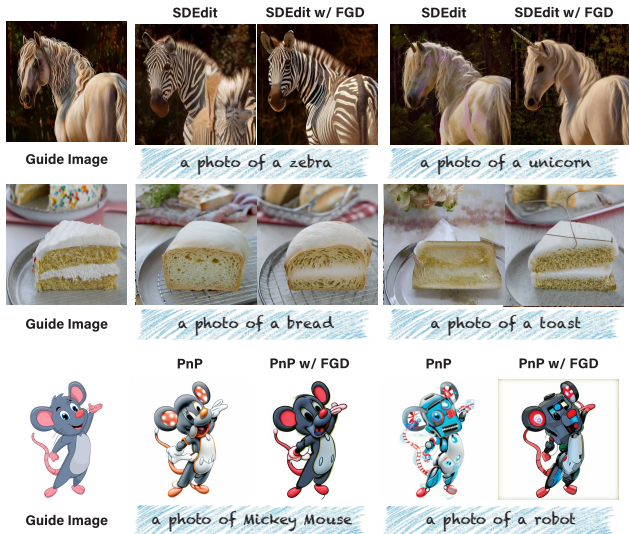


Figure 9: **FGD as a Lightweight Plug-In** The technique of our method is parallel with many existing I2I diffusion-based methods and thus FGD can be plugged into them to further control the strength of imposing structure information from the guide image.

7.2. Limitations

When designing this approach we took care to ensure that guided inputs to our network had variance similar to the training distribution. However, there is no guarantee that a supplied guide image will have structure that is in-distribution for the network, or that in-distribution images with the supplied structure will be able to satisfy other ob-

jectives (e.g., a text prompt). This is most noticeable when the given objective makes explaining the guide structure difficult. When the filter strength is set to be high (i.e., δ is very low) the likelihood of this happening increases, as the notion of structure becomes much more specific. In practice this can lead to over-smoothing, and in extreme cases slight halos in the shape of the guide image.

The use of a simple linear filter in FGD also lacks understanding of semantics in an image. This can lead to results that preserve the overall geometric structure of the guide image, but with different meaning to different parts. For example, in Fig. 11, decreasing the filter strength eventually causes a portrait of a face to turn into a portrait of a body with a similar silhouette to the guide image. Here, architecture-aware approaches would have a fundamental advantage over black-box methods like FGD if the goal is to preserve the original semantics of a face portrait, since internal features of the network may capture some of this information, making it possible to incorporate in the notion of guide structure.

7.3. Conclusion

This work presents a simple, efficient, and general approach to guiding diffusion models. Our work achieves results that are much closer to state-of-the-art architecture-specific methods while treating the diffusion network as a black box, and can easily be combined with others methods to allow finer control of structure guidance. These qualities make it a convenient and fast add-on to diffusion-based applications looking to add image-based control.

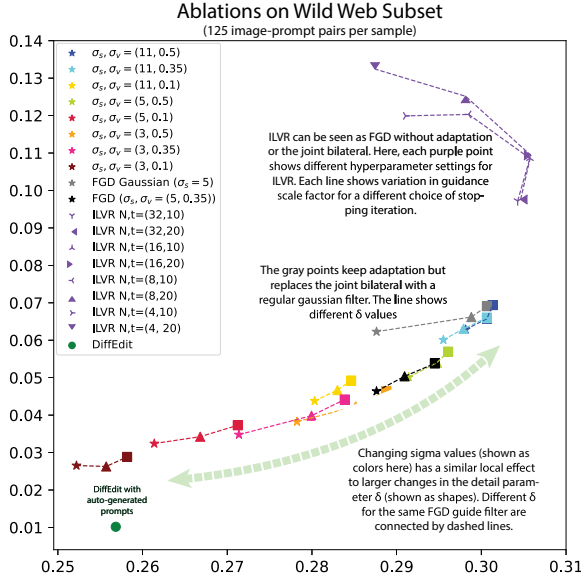


Figure 10: **Ablations** On a 125 image-text pair subset of Wild Web, we compare results of using bilateral filter with combinations of spatial standard deviation 3, 5, 11 and value standard deviation 0.1, 0.35, 0.5. We also compare with variations of ILVR [4], which could on a high level be understood as replacing our bilateral filter with a gaussian filter. Following the original paper, we set downsampling factor N to be 4, 8, 16, and 32, and the conditioning step range to be 10 and 20. We also show the result of DiffEdit [6] with auto-generated prompts via BLIP [16]. As in Fig. 8, the star, triangle, and square of the same color represent respectively results with δ value 0.05, 0.2, 0.5 under the same setup.

References

- [1] Mahmoud Afifi, Marcus A Brubaker, and Michael S Brown. Histogram: Controlling colors of gan-generated and real images via color histograms. In *Proceedings of the IEEE/CVF conference on computer vision and pattern recognition*, pages 7941–7950, 2021.
- [2] Peter J. Burt and Edward H. Adelson. *The Laplacian Pyramid as a Compact Image Code*, page 671–679. Morgan Kaufmann Publishers Inc., San Francisco, CA, USA, 1987.
- [3] Tao Chen, Ming-Ming Cheng, Ping Tan, Ariel Shamir, and Shi-Min Hu. Sketch2photo: Internet image montage. *ACM transactions on graphics (TOG)*, 28(5):1–10, 2009.
- [4] Jooyoung Choi, Sungwon Kim, Yonghyun Jeong, Youngjune Gwon, and Sungroh Yoon. Ilvr: Conditioning method for denoising diffusion probabilistic models, 2021.
- [5] Yunjey Choi, Youngjung Uh, Jaejun Yoo, and Jung-Woo Ha. Stargan v2: Diverse image synthesis for multiple domains.



Figure 11: **Limitations:** FGD guides a purely signal-based notion of structure that does not understand the semantics of an image. We can see this, for example, when a text prompt tends toward images with different composition from our guide image. Here, the prompt “a portrait of a lady on fire” transitions from a portrait of a woman’s face to that of a standing woman with a silhouette that looks roughly like the guide image. This is an advantage for architecture-aware methods, which have access to network features that carry more of this information.

In *Proceedings of the IEEE/CVF conference on computer vision and pattern recognition*, pages 8188–8197, 2020.

- [6] Guillaume Couairon, Jakob Verbeek, Holger Schwenk, and Matthieu Cord. Diffedit: Diffusion-based semantic image editing with mask guidance. *arXiv preprint arXiv:2210.11427*, 2022.
- [7] Elmar Eisemann and Frédo Durand. Flash photography enhancement via intrinsic relighting. *ACM Trans. Graph.*, 23(3):673–678, aug 2004.
- [8] David J. Field. Relations between the statistics of natural images and the response properties of cortical cells. *J. Opt. Soc. Am. A*, 4(12):2379–2394, Dec 1987.
- [9] Amir Hertz, Ron Mokady, Jay Tenenbaum, Kfir Aberman, Yael Pritch, and Daniel Cohen-Or. Prompt-to-prompt image editing with cross attention control. *arXiv preprint arXiv:2208.01626*, 2022.
- [10] Jonathan Ho, Ajay Jain, and Pieter Abbeel. Denoising diffusion probabilistic models. *Advances in Neural Information Processing Systems*, 33:6840–6851, 2020.
- [11] Phillip Isola, Jun-Yan Zhu, Tinghui Zhou, and Alexei A Efros. Image-to-image translation with conditional adversarial networks. *CVPR*, 2017.

- [12] Tero Karras, Timo Aila, Samuli Laine, and Jaakko Lehtinen. Progressive growing of gans for improved quality, stability, and variation. *arXiv preprint arXiv:1710.10196*, 2017.
- [13] Tero Karras, Samuli Laine, and Timo Aila. A style-based generator architecture for generative adversarial networks. In *Proceedings of the IEEE/CVF conference on computer vision and pattern recognition*, pages 4401–4410, 2019.
- [14] Bahjat Kawar, Shiran Zada, Oran Lang, Omer Tov, Huiwen Chang, Tali Dekel, Inbar Mosseri, and Michal Irani. Imagic: Text-based real image editing with diffusion models. In *Proceedings of the IEEE/CVF Conference on Computer Vision and Pattern Recognition*, pages 6007–6017, 2023.
- [15] Gihyun Kwon and Jong Chul Ye. Diffusion-based image translation using disentangled style and content representation. *arXiv preprint arXiv:2209.15264*, 2022.
- [16] Junnan Li, Dongxu Li, Caiming Xiong, and Steven Hoi. Blip: Bootstrapping language-image pre-training for unified vision-language understanding and generation. In *International Conference on Machine Learning*, pages 12888–12900. PMLR, 2022.
- [17] Luping Liu, Yi Ren, Zhijie Lin, and Zhou Zhao. Pseudo numerical methods for diffusion models on manifolds. *arXiv preprint arXiv:2202.09778*, 2022.
- [18] Chenlin Meng, Yang Song, Jiaming Song, Jiajun Wu, Jun-Yan Zhu, and Stefano Ermon. Sdedit: Image synthesis and editing with stochastic differential equations. *arXiv preprint arXiv:2108.01073*, 2021.
- [19] Alex Nichol, Prafulla Dhariwal, Aditya Ramesh, Pranav Shyam, Pamela Mishkin, Bob McGrew, Ilya Sutskever, and Mark Chen. Glide: Towards photorealistic image generation and editing with text-guided diffusion models. *arXiv preprint arXiv:2112.10741*, 2021.
- [20] Aude Oliva, Antonio Torralba, and Philippe G. Schyns. Hybrid images. *ACM Trans. Graph.*, 25(3):527–532, jul 2006.
- [21] Taesung Park, Alexei A Efros, Richard Zhang, and Jun-Yan Zhu. Contrastive learning for unpaired image-to-image translation. In *Computer Vision–ECCV 2020: 16th European Conference, Glasgow, UK, August 23–28, 2020, Proceedings, Part IX 16*, pages 319–345. Springer, 2020.
- [22] Gaurav Parmar, Yijun Li, Jingwan Lu, Richard Zhang, Jun-Yan Zhu, and Krishna Kumar Singh. Spatially-adaptive multilayer selection for gan inversion and editing. In *Proceedings of the IEEE/CVF Conference on Computer Vision and Pattern Recognition*, pages 11399–11409, 2022.
- [23] Gaurav Parmar, Krishna Kumar Singh, Richard Zhang, Yijun Li, Jingwan Lu, and Jun-Yan Zhu. Zero-shot image-to-image translation. *arXiv preprint arXiv:2302.03027*, 2023.
- [24] Georg Petschnigg, Richard Szeliski, Maneesh Agrawala, Michael Cohen, Hugues Hoppe, and Kentaro Toyama. Digital photography with flash and no-flash image pairs. *ACM Trans. Graph.*, 23(3):664–672, aug 2004.
- [25] Alec Radford, Jong Wook Kim, Chris Hallacy, Aditya Ramesh, Gabriel Goh, Sandhini Agarwal, Girish Sastry, Amanda Askell, Pamela Mishkin, Jack Clark, et al. Learning transferable visual models from natural language supervision. In *International conference on machine learning*, pages 8748–8763. PMLR, 2021.
- [26] Aditya Ramesh, Prafulla Dhariwal, Alex Nichol, Casey Chu, and Mark Chen. Hierarchical text-conditional image generation with clip latents. *arXiv preprint arXiv:2204.06125*, 2022.
- [27] Robin Rombach, Andreas Blattmann, Dominik Lorenz, Patrick Esser, and Björn Ommer. High-resolution image synthesis with latent diffusion models. In *Proceedings of the IEEE/CVF Conference on Computer Vision and Pattern Recognition*, pages 10684–10695, 2022.
- [28] Chitwan Saharia, William Chan, Saurabh Saxena, Lala Li, Jay Whang, Emily Denton, Seyed Kamyar Seyed Ghasemipour, Burcu Karagol Ayan, S Sara Mahdavi, Rapha Gontijo Lopes, et al. Photorealistic text-to-image diffusion models with deep language understanding. *arXiv preprint arXiv:2205.11487*, 2022.
- [29] Jiaming Song, Chenlin Meng, and Stefano Ermon. Denoising diffusion implicit models. *arXiv preprint arXiv:2010.02502*, 2020.
- [30] Antonio Torralba and Aude Oliva. Statistics of natural image categories. *Network: Computation in Neural Systems*, 14:391 – 412, 2003.
- [31] Narek Tumanyan, Omer Bar-Tal, Shai Bagon, and Tali Dekel. Splicing vit features for semantic appearance transfer. In *Proceedings of the IEEE/CVF Conference on Computer Vision and Pattern Recognition*, pages 10748–10757, 2022.
- [32] Narek Tumanyan, Michal Geyer, Shai Bagon, and Tali Dekel. Plug-and-play diffusion features for text-driven image-to-image translation. *arXiv preprint arXiv:2211.12572*, 2022.
- [33] Narek Tumanyan, Michal Geyer, Shai Bagon, and Tali Dekel. Plug-and-play diffusion features for text-driven image-to-image translation. *arXiv preprint arXiv:2211.12572*, 2022.
- [34] Tianyi Wei, Dongdong Chen, Wenbo Zhou, Jing Liao, Weiming Zhang, Lu Yuan, Gang Hua, and Nenghai Yu. A simple baseline for stylegan inversion. *arXiv preprint arXiv:2104.07661*, 9:10–12, 2021.
- [35] Lvmin Zhang and Maneesh Agrawala. Adding conditional control to text-to-image diffusion models. *arXiv preprint arXiv:2302.05543*, 2023.
- [36] Jun-Yan Zhu, Taesung Park, Phillip Isola, and Alexei A Efros. Unpaired image-to-image translation using cycle-consistent adversarial networks. In *Computer Vision (ICCV), 2017 IEEE International Conference on*, 2017.